Bioorganic & Medicinal Chemistry Letters 25 (2015) 3654–3657

Contents lists available at ScienceDirect

Bioorganic & Medicinal Chemistry Letters

journal homepage: www.elsevier.com/locate/bmcl

3-Hydroxy-4-pyridinone derivatives designed for fluorescence studies to determine interaction with amyloid protein as well as cell permeability

Maria A. Telpoukhovskaia, Jacqueline F. Cawthray, Cristina Rodríguez-Rodríguez, Lauren E. Scott, Brent D. G. Page, Brian O. Patrick, Chris Orvig *

Medicinal Inorganic Chemistry Group, Department of Chemistry, University of British Columbia, 2036 Main Mall, Vancouver, BC V6T 1Z1, Canada

ARTICLE INFO

Article history:
Received 26 March 2015
Revised 12 June 2015
Accepted 15 June 2015
Available online 23 June 2015

Keywords:
Metal chelator
Amyloid-beta
TD-DFT
bEnd.3
Fluorescent tracker

ABSTRACT

Finding a cure for Alzheimer's disease is an urgent goal. Multifunctional metal binders are used to elucidate its pathological features and investigated as potential therapeutics. The use of physicochemical and TD-DFT calculations constituted successful strategy in the design of 1-(4-(benzo[*d*]oxazol-2-yl)phenyl)-3-hydroxy-2-methylpyridin-4(1*H*)-one (**HL$_{21}$**) and 1-(4-(benzo[*d*]thiazol-2-yl)phenyl)-3-hydroxy-2-methylpyridin-4(1*H*)-one (**HL$_{22}$**). We report the synthesis and full characterization of these compounds, including X-ray crystallography. Using fluorescent signal as the readout, it was determined that **HL$_{22}$** interacts with amyloid-beta protein fibrils, and permeates into bEnd.3 cells used as a mimic of the blood–brain barrier. This provides the first example of direct investigation of our hydroxypyridinone compounds within a biological setting.

Solving neurodegenerative diseases (e.g. Alzheimer's disease (AD)) is one of the highest priority goals due to the rapid increase in the number of people affected. Recently, it was pointed out that AD may be behind a much greater number of deaths,[1] making discovery of its cure ever more urgent. While the causes of AD are not completely understood, theories that are used to guide drug discovery include the involvement of amyloid-beta (Aβ) protein, increased amounts of reactive metal ions Cu(II), Zn(II), and Fe(III), depletion of neurotransmitter acetylcholine, and increased oxidative stress; these are typically used in combination to afford multifunctional compounds.[2–4]

Among the first compounds to be studied for the potential use as AD therapeutics in our research group were repurposed 3-hydroxy-4-pyridones (HPOs) **Hdpp** and **Hppp**[5] (Fig. 1), whose metal binding affinities were previously established (e.g. **Hppp** binding to In(III), Al(III), and Ga(III) reported in 1991[6]). The proof of concept experiments involved antioxidant activity, studies with Aβ, and brain uptake.[5] As it had been established that the metal binding affinity of the HPO family is unaffected by the introduction of varying *N*-substituents, different groups were inserted into the scaffold to influence other properties of these compounds.[7] For instance, a linker approach was used to provide more flexibility to the aryl substituents, for example, transforming **Hppp** into **Hnbp**[8] (Fig. 1). The following generation of compounds included benzothiazole and benzoxazole functionalities in their structure in order to facilitate Aβ binding (e.g., **HL$_4$** and **HL$_5$**,[9] in addition to **HL$_{11}$** and **HL$_{12}$**[10] that included the methylene linker (Fig. 1)). These molecular scaffolds are found in in vivo amyloid imaging PET (positron emission tomography) tracers such as [^{11}C]-Pittsburgh Compound B (PIB) and [^{11}C]-BF-227.[11]

The shortcoming of the compounds from the second-generation library was that their interaction with biological systems could not be studied directly by conventional spectroscopic methods due to the high energy needed for their excitation. For this body of work, the methylene linker of **HL$_{11}$** and **HL$_{12}$** is replaced with a phenyl linker, which serves two purposes. First, the compounds more closely resemble parent compound PIB, and, secondly, this may allow for improved compatibility with spectroscopic methods used with protein and cell assays. Thus, the two novel pro-ligands that were designed are **HL$_{21}$** and **HL$_{22}$** (Fig. 1).

In designing compounds, potential interactions within biological systems must be considered. Lipinski's rules are a set of guidelines based on data available for the drugs on the market. These rules aim to achieve a balance between water and lipid solubility that increases the likelihood that a compound is bioavailable.[12] For a majority of drugs, the molecular weight is <500, *c*log*P* <5, and number of hydrogen donor and acceptor atoms are <5 and

* Corresponding author. Tel.: +1 604 822 4449; fax: +1 604 822 2847.
E-mail address: orvig@chem.ubc.ca (C. Orvig).

http://dx.doi.org/10.1016/j.bmcl.2015.06.059
0960-894X/

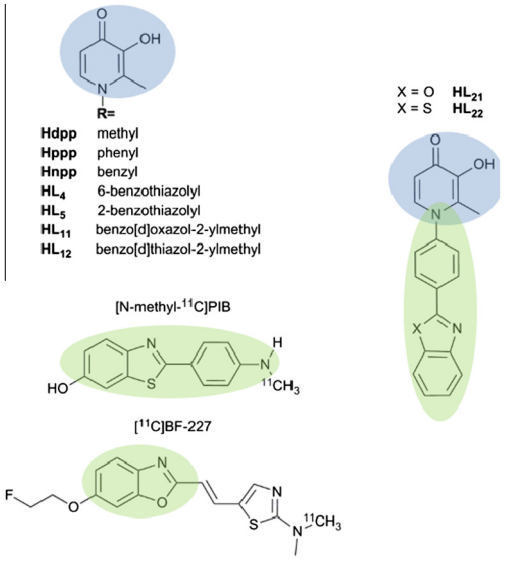

Figure 1. Previously studied HPOs from our work for potential use in AD, positron emission tomography tracers PIB and BF-227 used for in vivo plaque imaging, and novel pro-ligands **HL_{21}**, and **HL_{22}**. The blue colour highlights the HPO core that includes the metal binding part, while the green colour highlights the Aβ binding functionalities.

<10, respectively. While many drugs fall outside these limits, Lipinksi's rules remain a useful first pass filter that can be applied to a theoretical library in order to arrive at a smaller set of compounds for synthesis, thus optimizing lab bench time and expense. As the chemical space consists of a myriad of potential molecules of interest, it is advantageous to filter out compounds that may have low bioavailability before embarking on the synthesis of a more manageable library.

Another concern is whether the molecule would pass through the blood–brain barrier (BBB) to reach the organ of interest (i.e., the brain). The log BB value (Eq. 1) may be used as a predictor of BBB permeability; compounds with calculated log BB values >0.3 are likely to enter the brain, while those with values <−1.0 are not likely to do so.[13] In this equation, TPSA is the topological polar surface area, which is an estimate of the sum of the areas of the polar molecules, and *c* log *P* is the calculated water–octanol partition coefficient, which is a measure of hydrophobicity. These values, and other parameters from Table 1, were calculated with software found at http://www.molinspiration.com. (It should be noted that in this case, the log *P* value is approximated with MiLog *P*).

$$\log BB = -0.0148\ TPSA + 0.152\ c\log P + 0.139 \quad (1)$$

The pro-ligands **HL_{21}** and **HL_{22}** comply with Lipinski's rules (Table 1). The title compounds have log BB values of −0.46 and −0.17 (Table 1), thus they may exhibit modest passive permeability through the BBB, and they are improved compared to those of the methyl-linked compounds **HL_{11}** and **HL_{12}** (−0.50 and −0.88, respectively),[10] due in part to increased lipophilicity. These calculations suggest that these compounds should be prepared.

HL_{21} and **HL_{22}** were synthesised using a two-step procedure that involves amine insertion and cyclisation[14,15] (Scheme 1), leading to the phenyl-linked benzoxazole and benzothiazole HPOs. These two pro-ligands were characterised by 1D and 2D ^{1}H, ^{13}C NMR spectroscopy (Figs. S.1–S.6), HRMS, IR spectroscopy, and EA. As well, single crystals of intermediate Hcpp and compounds **HL_{21}** and **HL_{22}** were analysed by X-ray crystallography (Fig. S.7). Crystal structure and refinement data, as well as selected bond lengths and angles can be found in Tables S.2 and S.3. There is a noticeable bend in the benzoxazole, likely due to packing effects as evinced by the torsion angles between C13–O3–C19–C18 at 3.5° and C13–N2–C14–C15 at 5.5°; in the analogous **HL_{11}**, the torsion angle is minimal, at less than 1.2°.[10] As well, the torsion is not present in the **HL_{22}** benzothiazole, with the angle C13–S1–C19–C18 at 1.8° and the C13–N2–C14–C15 angle at 0.9°.

In our previous work, the compound **HL_{11}** was characterised by UV–vis and TD-DFT calculations. Because the compound absorbs at 280 nm under aqueous conditions, the use of a reporter molecule ThT was necessary to study its interaction with Aβ by conventional spectroscopic methods.[10] In this work we continue with our assessment of TD-DFT for predicting the electronic spectrum of small organic ligands; in particular, we were looking for a shift of the excitation wavelength to lower energy so that we would be able to detect directly compounds **HL_{21}** and **HL_{22}** in biological studies. In this study, **HL_{21}** was chosen for analysis to directly compare the phenyl-linked benzoxazole to the methylene-linked **HL_{11}**. Firstly, the electronic structure of **HL_{21}** was optimised at the B3LYP/6-31+g(d,p) level of theory. The DFT-calculated structure matches the solid state structure with the exception of the rotation of the phenyl substituent in relation to the main HPO ring. This difference arises from the packing effects that constrain the molecule in the solid state.

The TD-DFT calculated excitation energies and oscillator strengths for the ligand, **HL_{21}**, are compared with the experimental spectra in Figure 2. The data presented in Figure 2A show that at the B3LYP level of theory using the 6-31+g(d,p) basis set, TD-DFT successfully predicts both the excitation energies and relative oscillator strengths of the electronic spectrum of **HL_{21}**. The predicted λ_{max} of 310 nm compares well with the experimental λ_{max} of 306 nm (recorded in water at pH 7).

In order to gain insight into the nature of the calculated electronic transitions, the molecular orbitals representing the transitions can be analyzed in terms of the occupied and virtual molecular orbitals (MOs). For **HL_{21}**, the theoretical spectrum is dominated by the excited state transition corresponding to λ_{max} 310 nm characterized by a single-electron transition from the HOMO-1 to the LUMO (Fig. S.8). There are also weakly allowed singlet excited states at 358.5 nm corresponding to the HOMO to LUMO (Fig. S.8) transition and at 262 nm attributed to HOMO to LUMO + 2 (Fig. S.8) transition (with 15% contribution from HOMO to LUMO + 1 (Fig. S.8)). All values are in good agreement with those obtained experimentally. Significant differences in the theoretical

Table 1
Lipinski's rules parameters and log BB calculated values for **HL_{21}** and **HL_{22}**

	HL_{21}	HL_{22}
MW	318.33	334.4
MiLog *P*	2.71	3.35
TPSA	68.27	55.13
HBA	5	4
HBD	1	1
Lipinski's rules	Pass	Pass
Log BB	−0.46	−0.17

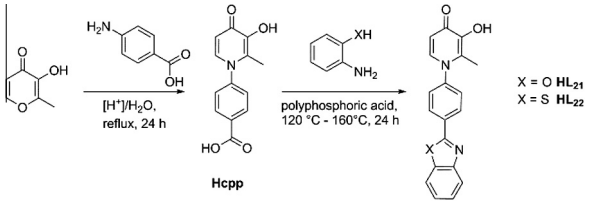

Scheme 1. **HL_{21}** and **HL_{22}** synthesis.